NON-EYRING TEMPERATURE DEPENDENCE OF DYNAMIC ISOTOPE EFFECTS

A Thesis

by

N. REBECCA RUIZ

Submitted to the Office of Graduate Studies of
Texas A&M University
in partial fulfillment of the requirements for the degree of

MASTER OF SCIENCE

December 2006

Major Subject: Chemistry

NON-EYRING TEMPERATURE DEPENDENCE

OF DYNAMIC ISOTOPE EFFECTS

A Thesis

by

N. REBECCA RUIZ

Submitted to the Office of Graduate Studies of
Texas A&M University
in partial fulfillment of the requirements for the degree of

MASTER OF SCIENCE

Approved by:

Chair of Committee,	Daniel A. Singleton
Committee Members,	Donald J. Darensbourg
	Kevin Burgess
	Perla B. Balbuena
Head of Department	David H. Russell

December 2006

Major Subject: Chemistry

ABSTRACT

Non-Eyring Temperature Dependence of Dynamic Isotope Effects.

(December 2006)

N. Rebecca Ruiz, B.S., Northwest Nazarene University

Chair of Advisory Committee: Dr. Daniel A. Singleton

Our group has recently described a new form of kinetic isotope effect that arises from dynamic selectivity in the bifurcation of a reaction pathway on the slope of an energy surface. Since the selection between products does not occur at a potential energy saddle point, we proposed that the isotope effect is decided by dynamic factors that are not necessarily related to zero point energy effects on the surface. As an alternative explanation, it has recently been suggested that variational transition state theory can account for these isotope effects. The dynamic explanation and variational transition state theory explanation make distinct predictions as to the temperature dependence of these isotope effects. I describe here my studies of the temperature dependence of the intramolecular isotope effects for the reaction of singlet oxygen with *gem*-tetramethylethylene-d_6. The selectivity observed for this reaction across a broad temperature range is clearly a non-Eyring distribution and thus the mechanism cannot be adequately described solely using transition state theory or even some variation of it. After using these results to evaluate competing theories it was concluded that this mechanism could only be properly understood using a dynamic explanation.

ACKNOWLEDGEMENTS

I would first like to acknowledge Doc because of his unwavering support of my academic pursuits and his dedication to research and education. Next comes all of the members of the Singleton Group that I worked with (and a few that came before), the lab owes it's unique and legendary character to each and every one of you. Thank-you to the members of the Aggie Christian Grads who were my life-support and family here in Aggieland, not to mention my fellow chemistry grad students with whom I've learned, taught, studied, worked, laughed, and cried.

I would like to say thank-you to my parents and family for a lifetime of support and love, particularly Mom, who taught me to read as a child and to cherish learning. I would especially like to acknowledge Wava, who taught me the principles of algebra and logic problems when I was little and later shared my pursuit of chemistry becoming my lab partner and study buddy in all of our undergraduate chemistry classes simply because that's what sisters do. Finally a lifetime of thanks to my dear husband, Louie, who won my heart and kept me going during the long haul of my last year in grad school.

TABLE OF CONTENTS

LIST OF FIGURES

FIGURE Page

LIST OF TABLES

CHAPTER I

INTRODUCTION

Transition State Theory

The understanding of the rates and selectivities of chemical reactions is predominantly based on transition state theory. Since its inception by Eyring, transition state theory has undergone many refinements to come to the various forms known and used today. Over time, transition state theory has passed from being a *model* for understanding chemical reactivity- to being *integral* to the way chemists look at all reactions themselves. This integration has become so tight that there are few outlets available for rationalization of reactions in which transition state theory fails to predict or explain the outcome.

Transition state theory relates the rates of reactions to the enthalpy and partition function of a transition state, which is a multidimensional surface dividing starting material from product. In thermodynamics terms, the rate of a reaction can be expressed as in eq 1, often referred to as the Eyring equation. In this equation k is the overall reaction rate, k_b is the Boltzmann constant, T is absolute temperature, h is Planck's constant, $-\Delta G^{o}_{act}$ is the standard Gibbs free energy of activation, R is the universal gas constant, $-\Delta H^{o}_{act}$ is enthalpy of activation, and $-\Delta G^{o}_{act}$ is entropy of activation. The symbol κ is the transmission coefficient, a correction for any recrossing of products across the dividing surface, and has a value ranging between 0 and 1.

This thesis follows the style of *Journal of the American Chemical Society*.

$$k = \kappa\left(\frac{k_b T}{h}\right)e^{-\Delta G^0_{act}/RT} = \kappa\left(\frac{k_b T}{h}\right)e^{-\Delta H^0_{act}/RT}e^{\Delta S^0_{act}/R} \quad (1)$$

Eq 1 can be used to relate the competitive rates of two (or more) reactions in the same system. The rate of one reaction (k) can easily be related to the rate of the other (k') by dividing the equations for each and canceling out identical constants, assuming that κ is identical for each. The relative rates can be interpreted as the differences in their free energies of activation, represented as $\Delta\Delta G^0_{act}$, as shown in eq 2. This equation can also be expanded to show that the individual rates are equivalently interpreted as the differences in their enthalpies and entropies of activation, $\Delta\Delta H^0_{act}$ and $\Delta\Delta S^0_{act}$, respectively (eq 3).

$$k = \kappa\left(\frac{k_b T}{h}\right)e^{-\Delta G^0_{act}/RT} \quad \text{and} \quad k' = \kappa\left(\frac{k_b T}{h}\right)e^{-\Delta G^0_{act}'/RT}$$

$$\frac{k}{k'} = \frac{e^{-\Delta G^0_{act}/RT}}{e^{-\Delta G^0_{act}'/RT}}$$

$$k/k' = e^{-\Delta\Delta G^0_{act}/RT} \quad (2)$$

$$k/k' = e^{-\Delta\Delta G^0_{act}/RT} = e^{-\Delta\Delta H^0_{act}/RT}e^{-\Delta\Delta S^0_{act}/R} \quad (3)$$

By utilizing this type of approach, the interpretation of rates and selectivity has a formalistic character that lends itself a degree of flexibility. Variations within a system are simply accounted for as variables of the base equation and can be applied to most situations; a most significant variation being the dependence of $\Delta\Delta H^0_{act}$ and $\Delta\Delta S^0_{act}$ on temperature.

A variety of predictions can be made using eq 3, particularly regarding the effect of temperature on selectivity. These predictions have been found to be most useful and qualitatively accurate for numerous situations. To be fair, allowing for temperature dependence in $\Delta\Delta H^0_{act}$ and $\Delta\Delta S^0_{act}$, eq 3 could account for almost any observations. However, a potentially breakable prediction significant to this work is the effect on selectivity as temperature (T) decreases significantly, approaching absolute 0. According to eq 3, selectivity should increase limitlessly as T is reduced to 0. An exception to this has been observed in reactions with large amounts of tunneling, but in such cases $\Delta\Delta H^0_{act}$ is exactly zero at sufficiently low temperatures.[1-8] Outside of such tunneling cases, the exponential effect of temperature on selectivity has been inviolate.

This traditional treatment of relative rates or product selectivity in a reaction associates the product ratios with the energy difference between the transition states leading to the two products. In such a treatment there is a subtle presupposition that separate products are always formed from separate transition states. The traditional modeling for the minimum energy pathway for the formation of each product could be displayed in a two-dimensional reaction coordinate diagram such as the one shown in Figure 1A. However, reality is multidimensional, and complications arise that are not well represented in two dimensions. One issue is that in three or more dimensions, a

transition state is not a maximum but a saddle point. This allows two transition states to be adjacent, while in two dimensions this is not possible. A second issue is that one transition state can lead to two or more products. Both of these possibilities can be understood by comparing the two-dimensional reaction coordinate diagram in Figure 1A to the energy surface displayed in Figure 1B. In Figure 1B, there are two adjacent transition states, and reactants passing the rate-limiting transition state at left can proceed downhill to two products.

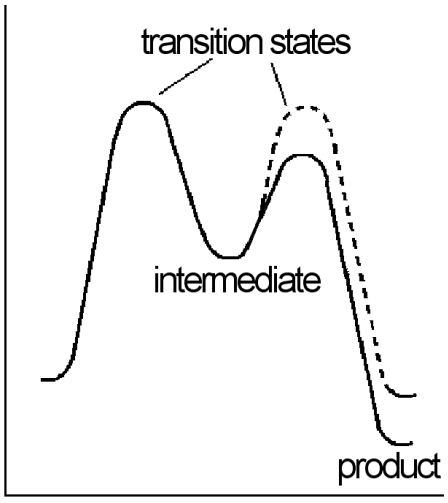

Figure 1A. 2-D Reaction coordinate diagram.

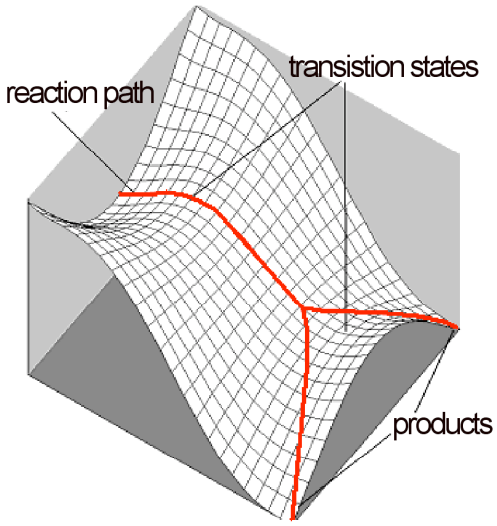

Figure 1B. 3-D Energy surface diagram.

Introduction to Dynamics

After coming to view reaction pathways as more like the three-dimensional potential energy surface just described, it becomes almost natural to question the basic assumption that separate products invariably arise from separate transition states. This assumption has been shown unreliable from a theoretical standpoint in a variety of

situations[9-19]. For example, Hase's ab initio quasiclassical trajectory studies of the cyclopropyl radical ring-opening gave evidence for both a conrotatory and disrotatory ring-opening as well as evidence of a valley ridge inflection point along the potential energy surface, a phenomenon which will be discussed in further detail below. Schlegel and Shaik's theoretical studies of ketyl anion radicals with alkyl halides predict a single transition state with a bifurcating pathway leading to both electron transfer and carbon-alkylated products.[18] In theoretical studies by Birney and coworkers, the formation of semibulvalene in deazitations involves sequential transition states along the minimum energy pathway as well as a valley ridge inflection point.[20]

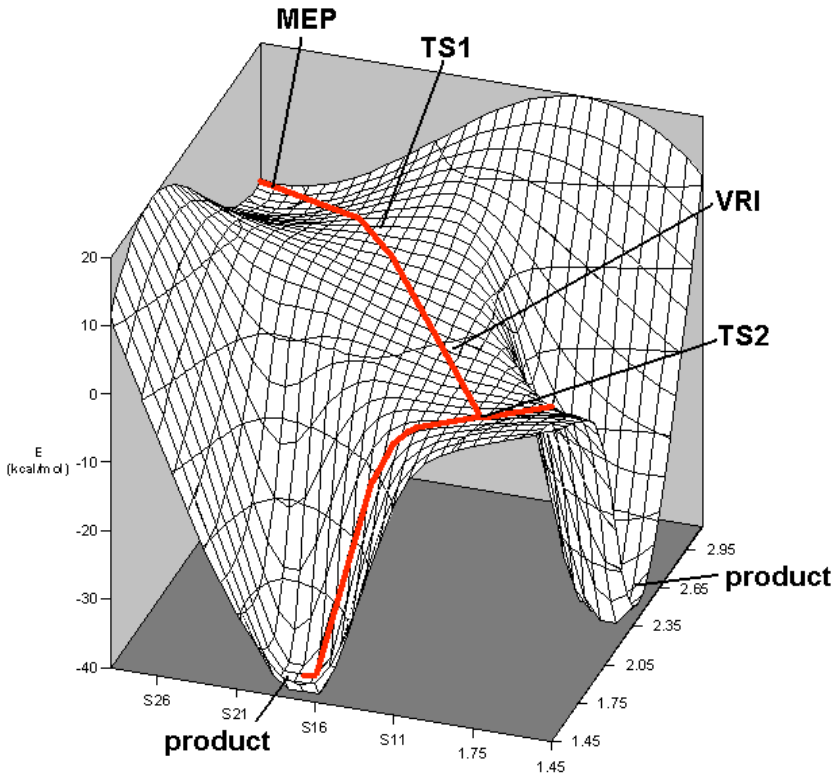

Figure 2. Potential energy surface of a bifurcating reaction pathway

In all of these examples, products of lower symmetry follow a symmetrical transition state. By necessity, a reaction path through such transition states must bifurcate as it breaks symmetry to form two (or more) products. Energy surfaces of this type, as in Figure 1B or Figure 2, are referred to as bifurcating energy surfaces. In such cases two saddle points sit adjacent to one another (TS1 and TS2), connected by the minimum energy pathway (MEP), and the area in between them is known as the valley-ridge inflection (VRI). It is at the VRI, that trajectories will begin to deviate towards their respective product valleys. These reactions are referred to as having a "two-step no intermediate mechanism" as there are two separately-affectable and so kinetically distinguishable steps, yet there is no minimum. The product selectivity is determined along the slope of the energy surface rather than at the transition state.[21]

It has been suggested by Singleton and coworkers that the ene reaction of alkenes with ($^1\Delta_g$) oxygen ($^1O_2$) involves a bifurcating energy surface of this type. In such a case as it was designed, the two products were only distinguishable by their differences in isotopic substitution so that the selectivity could be quantitatively represented as an intramolecular kinetic isotope effect (KIE).[21-24] Singleton proposed that the observed isotopic selectivity reflected a new type of KIE, best understood by dynamic trajectories. The evidence that brought him to this conclusion is more fully described later in this work.

This thesis describes an extensive experimental study of the ene reaction of $^1O_2$. In this study, gem-tetramethylethylene-d_6 (TME-d_6) was synthesized and subjected to standard $^1O_2$ conditions at a wide range of temperatures. The mixture of products at each

temperature, only distinguishable by isotopic substitution, was used to determine, in effect, the intramolecular KIE. These results were studied in conjunction with theoretically predicted isotope effects, within the same general temperature range, based on trajectory calculations. The temperature dependence of the selectivity was found to be determinedly non-Eyring in nature and as such is a unique case, experimentally. The experimental results were found to be reasonably predictable when examined in the manner as previously described by Singleton. Neither conventional nor variational transition state theory was able to predict the selectivity as aptly.

Dynamic effects have partially resolved the mechanistic debate over several reactions and have clarified the mysterious regioselectivity and isotopic selectivity as well.[21,24-30] It has been suggested that reactions following a two-step no intermediate mechanism are far from anomalous, but are commonly mischaracterized as concerted processes.[24] Since reactions have typically been looked at in terms of either one-step concerted mechanism or a two-step mechanism, new investigations must be undertaken to qualitatively understand selectivity in these reactions.

History of the Ene Reaction of Singlet Oxygen

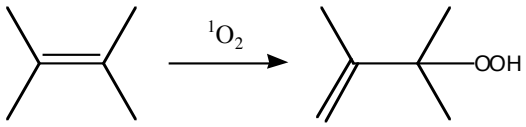

1 **2**

Figure 3. The $^1O_2$ ene reaction of tetramethylethylene.

The mechanism of the ene reaction of $^1O_2$ with small alkenes, such as tetramethylethylene **1** (see Figure 3), has been explored extensively.[31-34] Although this reaction is formally an allowed pericyclic process that could proceed by a transition state resembling **3** (see Figure 4), intermolecular isotope effects have shown that this is not a realistic mechanistic explanation. A competitive reaction between tetramethylethylene and tetramethylethylene-d_{12}, conducted by Stephenson and coworkers, exhibited an intermolecular isotope effect of only 1.11. This observation indicates that hydrogen transfer does not occur during the rate-determining step, consequently ruling out the concerted mechanism previously proposed. In standard mechanistic analysis, this forces the conclusion that there is an intermediate in the mechanistic process. Several possible intermediates can be reasonably proposed, such as a zwitterionic or diradical **4**, perepoxide **5**, or exciplex **6** intermediate (see Figure 4), however more experimental evidence was required to narrow down the field of possibilities.

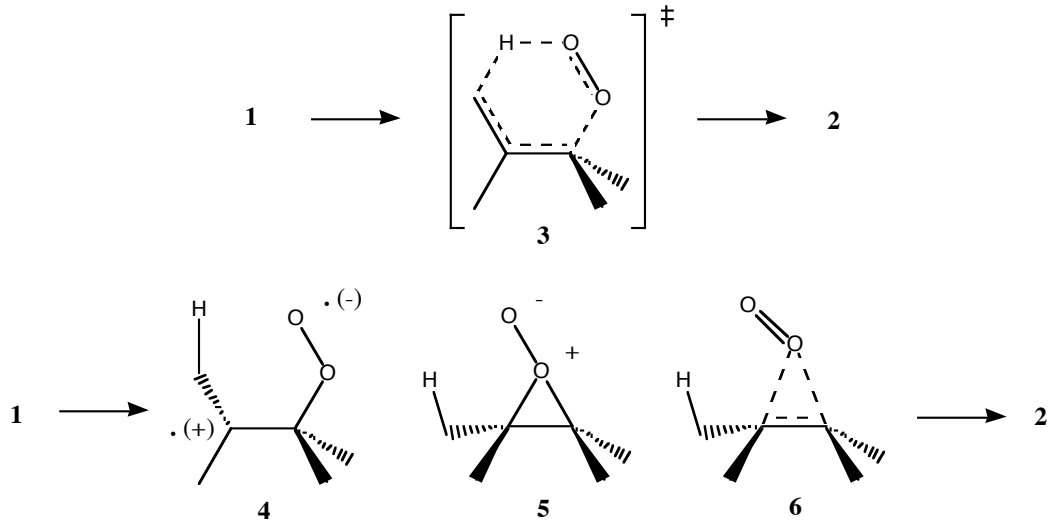

Figure 4. Previously proposed intermediates for the $^1O_2$ reaction of tetramethylethylene.

Stephenson and coworkers utilized a variety of deuterium labeled alkenes to obtain a series of KIEs for the reaction of $^1O_2$ with each, the results of which are shown in Figure 5. His observations led to a more expansive understanding of the mechanism. The isomers, **7** and **9,** showed significant intramolecular isotope effects ranging from 1.38 to 1.41, whereas isomer **8** exhibited only a small effect of 1.04-1.09. The isomer **10**, similarly studied by Foote, was observed to also have a large isotope effect of 1.38, comparable to **7** and **9**.

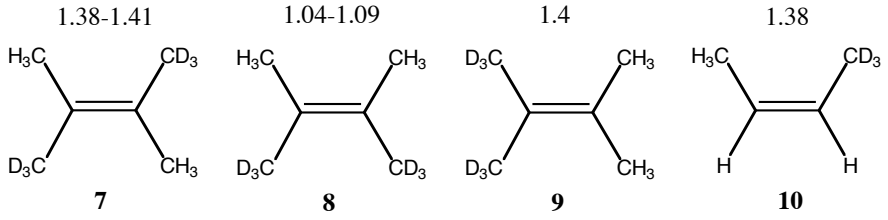

Figure 5. Intramolecular isotope effects on deuterium labeled olefins.

A zwitterionic or diradical intermediate is consequently ruled out by these results, as they would both be expected to have large observed isotope effects with **7** and **8**, but not with **9** and **10**. After rate-limiting formation of the zwitterionic or diradical intermediate resulting from **7** or **8** (see Figure 6), the intermediate would select between the proteomethyl and deuteriomethyl in the product forming step, a selection unavailable in the **9** and **10** intermediates.

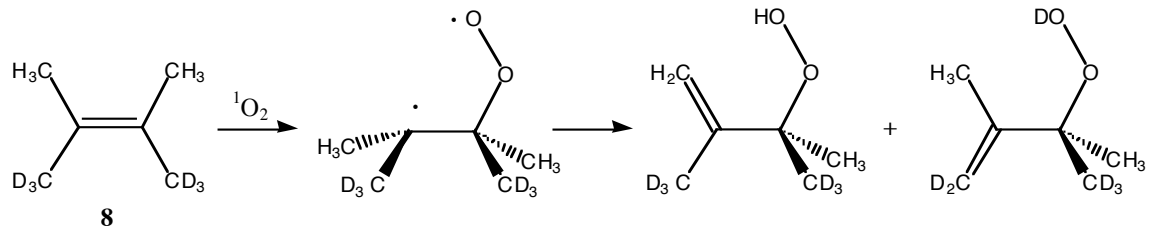

Figure 6. Product mixture expected from mechanism including a diradical intermediate.

A perepoxide or exciplex intermediate is much more consistent with the observed isotope effects in that both would be expected to have large observed isotope effects with **7**, **9**, and **10**, but not with **8**. After rate-limiting formation of the perepoxide or exciplex intermediate resulting from **7**, **9** (see Figure 7), and **10**, the intermediate would select between the proteomethyl and deuteriomethyl in the product forming step, a selection unavailable this time in the **8** intermediate. Consequently it was concluded that the intermediate must be a perepoxide or exciplex type intermediate.

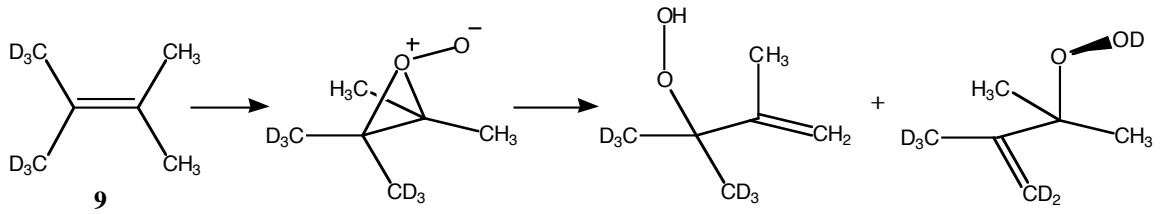

Figure 7. Product mixture expected from mechanism including a perepoxide intermediate.

In contrast, a variety of theoretical calculations performed by Singleton and coworkers predicted several different mechanisms, standard high level methods did not support a perepoxide or exciplex type intermediate, and were unable to adequately

predict the experimental results previously described. They then sought to further investigate the mechanism experimentally by obtaining both intermolecular and intramolecular ^{13}C isotope effects, gaining a more detailed picture of the structure of the rate-limiting transition state. The intermolecular ^{13}C KIEs of a nearly-symmetrical alkene **11** (see Figure 8) reacted with $^1O_2$ were observed at natural abundance using high resolution NMR techniques in analogy with processes designed and utilized previously by Singleton and coworkers.[35] Similarly small isotope effects were observed at each olefinic carbons in the recovered starting material **11** indicating a symmetrical approach of the oxygen to olefin bond.

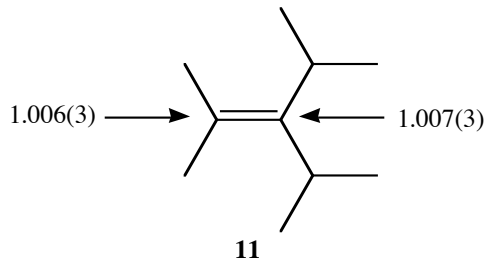

11

Figure 8. ^{13}C isotope effects for the $^1O_2$ reaction with **11**.

Intramolecular ^{13}C KIEs were observed by isolating the product of $^1O_2$ with tetramethylethylene at natural abundance and obtaining the relative integrations of the ^{13}C signals. When analyzed in the light of each mechanistic model previously proposed, the concerted and diradical mechanisms were even more fully excluded and it was shown that a species with perepoxide type symmetry occurs after the rate-limiting step.

Next, Singleton and coworkers pursued a variety of theoretical calculations and found two contiguous transition states, TS1 and TS2, with no intermediate, much like the potential energy surface seen in Figure 2. On this surface the product determining selectivity occurs at the VRI, before the reacting species reaches TS2 (see Figure 9). They employed quasiclassical direct dynamics calculations, closely modeling the potential energy surface along the pathway where the O_2 is approaching the olefin.

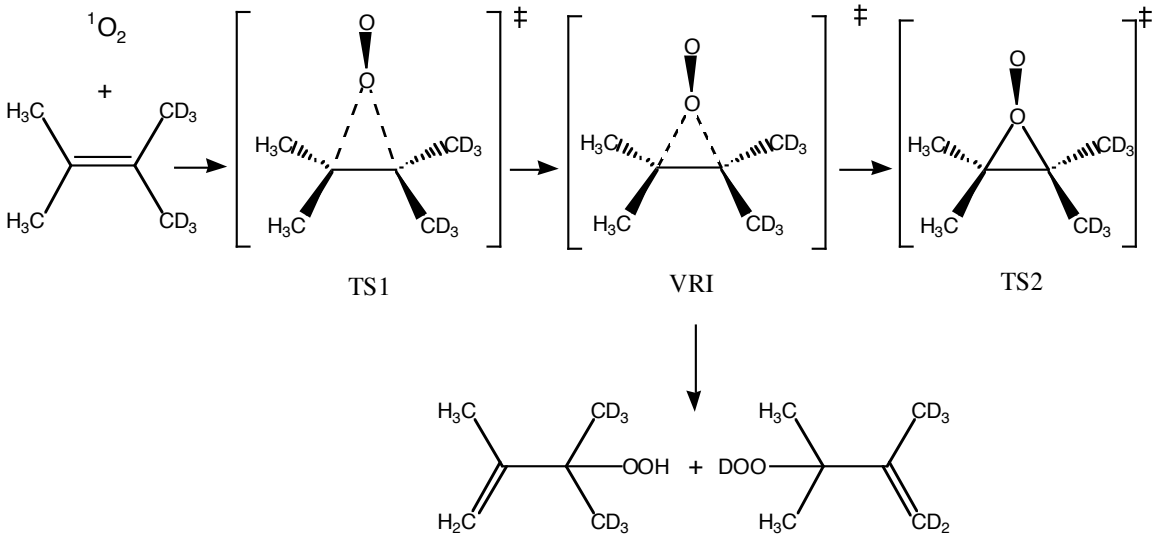

Figure 9. Two-step no intermediate mechanism of ene reaction $^1O_2$ with TME-d_6 as proposed by Singleton

Each trajectory was initialized with a geometry in between TS1 and the VRI, centered on the MEP of a symmetrical potential energy surface and thus unbiased towards the reaction of hydrogen versus deuterium. However, at both 0 K and 263 K the trajectories followed favored reaction with hydrogen. At 0 K, 183 trajectories afforded a k_H/k_D of 2.0. At 263 K, 257 trajectories afforded a k_H/k_D of 1.38, closely matching the

experimental value. Although not a quantitatively accurate manner of predicting KIEs, Singleton ascertained that this demonstrates that dynamically based selectivity can occur along a symmetrical barrierless energy surface forming a new type of isotope effect that is unrelated to typical zero point energy effects.

In 2004 Lluch and coworkers challenged the claim that dynamic effects were the source of selectivity for the ene reaction of singlet oxygen and asserted his own claims that the variational transition state theory (VTST) is sufficient to explain the KIEs at variable temperatures.[36] VTST differs from traditional transition state theory by accounting for recrossing of the reactants across the reaction barrier, a notable assumption inherent in conventional TST. Lluch attempted to make his calculations comparable to Singleton's by employing the same basis set and level of theory. From the valley ridge inflection geometry he found a bifurcation in the minimum energy pathway leading to two distinct pathways, one for the hydrogen abstraction and the other for the deuterium abstraction. Along each of these pathways he calculated a dynamical bottleneck and determined it to be the true source of selectivity. From these findings, Lluch calculated several intramolecular KIEs between 150 and 500 K, which in turn predicted a traditional Eyring shaped curve where the selectivity increases rapidly as the temperature decreases (Figure 10). At the time of his work, no experimental evidence on the temperature dependence of the reaction was available to compare to.

Our hypothesis and the subject of this thesis is that the intramolecular isotopic selectivity in these reactions constitutes a new form of kinetic isotope effect, and as such, it is of fundamental interest to observe the basic characteristics of a new phenomenon. Does the temperature dependence of the selectivity differ from that normally observed for

reactions in which the products arise from separate transition states? Can the selectivity be modeled by an Eyring relationship as in eq 3? Although the Lluch variational transition state theory treatment errs quantitatively, can it qualitatively account for the temperature dependence of the isotope effect? By answering this last question, we hoped to definitively decide whether variational transition state theory is really applicable to these reactions. Can trajectory calculations account for the temperature dependence of the isotope effect? If so, can this be used to gain insight into observations? Overall, our goal being to observe, theoretically predict, and understand the temperature dependence of the isotope effect in these reactions. We have largely succeeded.

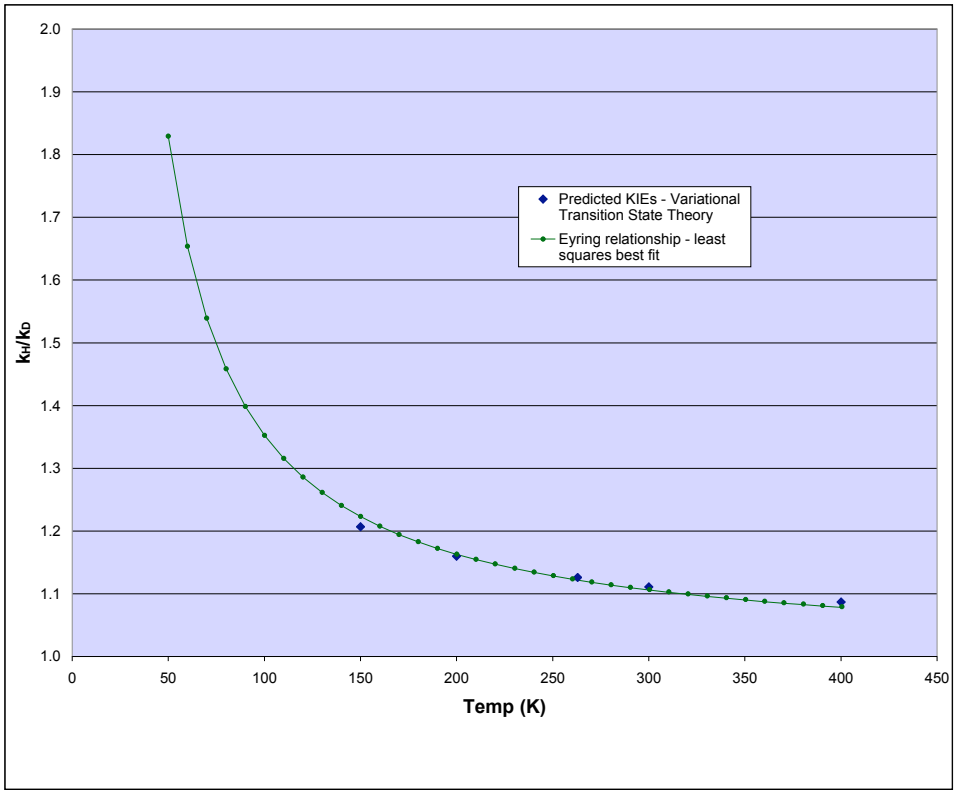

Figure 10. Lluch's VTST predictions compared to an Eyring curve.

CHAPTER II

RESULTS

Experimental Isotope Effects

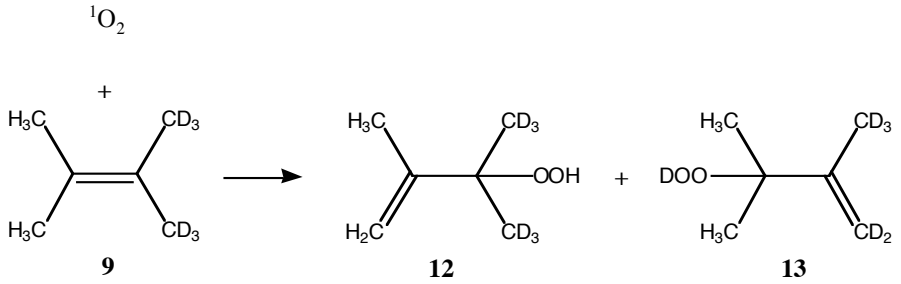

Figure 11. $^1O_2$ reaction of tetramethylethylene-d_6 to form a hydroperoxide mixture.

The principal reaction chosen for study is the $^1O_2$ ene reaction of tetramethylethylene-d_6 **(9)** (see Figure 11), chosen because it is a key example used in the previous studies by Singleton and Lluch. Also, the substrate is easily synthesized (see Figure 12) through a three-step process, adapted from the procedure of Adam and coworkers.[37]

The reaction of **9** to form the hydroperoxide mixture of **12** and **13**, as shown in Figure 13, was performed on a 100-200 mg scale in methanol or a methanol mixture solvent system using Rose Bengal as a sensitizer. The reaction was taken to partial completion in order to obtain quantitatively reliable KIE by limiting the possibility of secondary or side reactions. The isomers in the product mixture are only differentiated by their isotopic arrangement enabling the measurement of the reaction selectivity. Since the mixture of products contains the limitedly stable hydroperoxides, they were immediately deoxygenated to form the alcohols **16** and **17** before analysis.

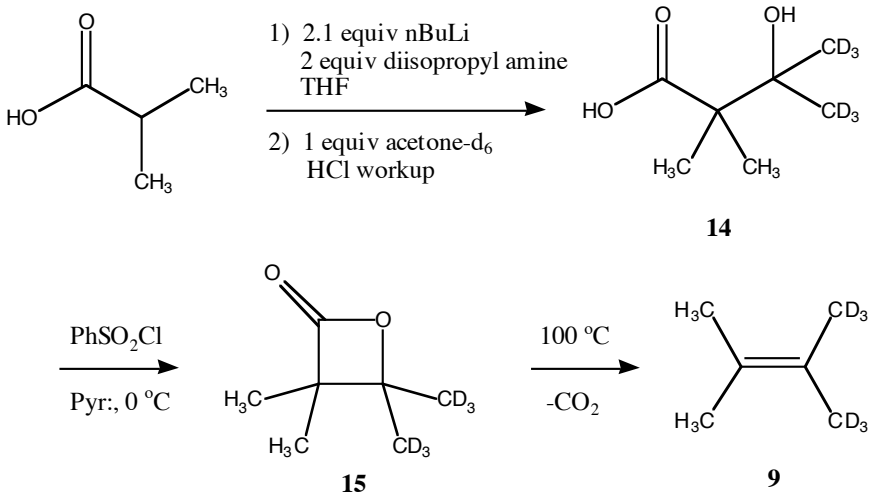

Figure 12. Synthesis of tetramethylethylene-d_6.

This conversion step has no effect on the isotopic composition of the products. At this point the mixture of products was isolated by extraction and purified by chromatography and distillation for NMR analysis. Multiple high resolution ^{1}H-NMRs of each sample were run back to back with standard non-deuterated samples reacted under the same conditions. The average of the integrations was used to determine the ratio of isotopomeric alcohols **16** and **17**. The integrations for all peaks were corrected using the average integrations from the standard sample, improving the quantitative accuracy of the integrations. In some cases baseline corrections were also employed. After correction, the methyl peaks of **17** were compared to the methyl and methylene peaks of **16**, which were then used to calculate the KIE for each sample. This method of measuring KIEs utilizing high resolution NMR is analogous to the methods developed by Singleton and coworkers to study a variety of chemical phenomena.

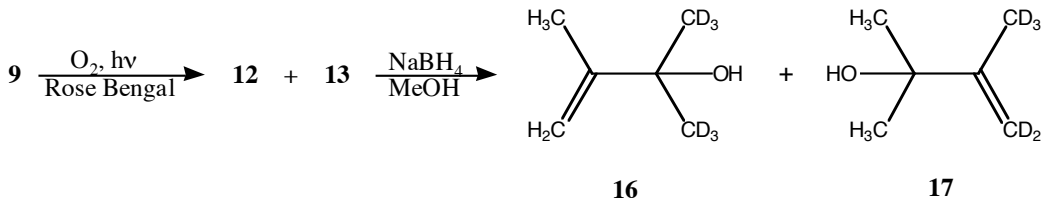

Figure 13. Conversion of tetramethylethylene to hydroperoxide mixture and subsequently to alcohol mixture for analysis.

As can be expected with a study spanning such a wide temperature range, some variation in reaction conditions was necessary. Great concern was given to keeping the differing systems as comparable as possible, so only the primary solvent was varied. For reactions at 193 K to 328 K, methanol was the only solvent used, whereas for reactions at 118 K to 163 K, a mixture of Freons, either $CHClF_2$ or 2:1 $CHClF_2$:CHF_2, with 5% methanol was used. A variety of other major solvents were tried in order to expand the temperature range (Table 1) before turning to Freon mixtures, but none were found to provide an adequate environment for significant reaction of $^1O_2$ or produced too many side reactions to be useful. Several reactions at 77 K were run using a solvent mixture of liquid nitrogen and 5% methanol suspended heterogeneously. Observed KIEs for each were found to be in reasonable agreement.

As is apparent in Table 1, many solvents systems were tried and rejected for various reasons. Much was learned from this process that made it possible to afford greater confidence to the comparability of the solvent systems finally chosen for the final study. Isolated non-polar solvents tended to inhibit reactivity almost completely, but with even a small amount of methanol normal reaction often transpired. In attempts to gain samples run at lower temperature, which are of particular interest, a variety of mixtures of

methanol with lower boiling solvents were tried. Several samples were acquired, however the quantity of side and/or secondary products from reaction with the non-polar solvent made them unreliable and useless for KIEs.

Table 1. Alternative solvent system attempts for expanding temperature range

Solvent	**T (K)**	**t (h)**	**rxn**
1,2-propanediol	298	2	-
1,2-propanediol	373	1	-
1:1 1-octanol/isopropanol	298	6	-
1:1 1-octanol/isopropanol	328	12.5	-
1:1 1-octanol/isopropanol	343	15	-
1:3 1-octanol/isopropanol	343	5	-
1:3 1-octanol/isopropanol	363	5	-
1-octanol	298	12	-
1-octanol	423	6	-
1-octanol	453	9	-
diethyl ether	183	2	-
diethyl ether	298	15.5	-
p-dioxane	298	4	-
p-dioxane	353	2	-
pentane	298	15.5	-
toluene	298	6	-
1:1 pentane/methanol	153	1	74%
1:3 pentane/methanol	173	1	43%
1:3 methanol/pentane	158	3	20%
1:10 methanol/pentane	298	3	10%
1:10 methanol/pentane	148	3	12%
1:1 methanol/diethyl ether	173	3	10%
1:3 methanol/diethyl ether	168	3	16%
1:10 methanol/diethyl ether	298	3	8%
1:10 methanol/diethyl ether	163	3	-
1:5 methanol/n-propanol	298	6	23%
1:5 methanol/2-methylbutane	298	6	30%
1:2:10 diethyl ether/pentane/methanol	183	2	18%
1:2:6 n-propanol/methylcyclohexane/pentane	298	6	-

Conversely, with Freon/methanol mixtures, no such side or secondary products were seen giving credence to the belief that the $^1O_2$ ene reaction with alkenes is undergoing the same mechanism as in the methanol only reactions. Table 2 lists the observed KIEs from this. The most notable qualitative observation with these KIEs is the leveling off of the effect seen as the temperature decreases, reaching a limiting isotope effect of approximately 1.56. Some scattering is noticeable in the data, but that is likely due to necessary variations in reaction conditions.

Table 2. Observed KIEs for the ene reaction of $^1O_2$ with *gem*-tetramethylethylene-d_6 at a variety of temperatures.

T (K)	KIE
75	1.559
75	1.595
118	1.566
138	1.586
158	1.545
163	1.530
193	1.538
208	1.548
218	1.464
248	1.456
276	1.417
298	1.373
313	1.326
328	1.300

As a simple means of observing KIEs in a different manner, a series of $^1O_2$ reactions with both tetramethylethylene and gem-tetramethylethylene-d_6 were attempted on an NMR scale in deuterated solvent systems, chloroform-d_3 and benzene-d_6. Preliminary results at room temperature were very inconsistent with known isotope effects, indicating a much higher k_H/k_D than observed previously. It was theorized that a

second mechanism, such as a radical type two oxidation, was occurring along with the $^1O_2$ reaction and a mixed KIE was ultimately being observed. This approach was discontinued, as it became no more useful than an interesting way of monitoring by-product formations.

Trajectory Studies

Extensive quasiclassical trajectories on the B3LYP/6-31G* surface of the ene reaction of $^1O_2$ with tetramethylethylene-d_6 were employed to study the temperature dependence of selectivity under this theoretical model in order to ascertain if it could adequately predict the obtained experimental results. Each trajectory was initialized with O_1-C_1 and O_1-C_2 distances of 1.95 Å, a geometry in between TS1 and the VRI, centered on the MEP of the B3LYP surface and thus unbiased towards the reaction of hydrogen versus deuterium in the same manner as the trajectories run by Singleton and coworkers. A linear sampling of possible displacements for each normal mode was used to randomize the starting atomic positions. More than 2000 trajectories were initialized at 0 K, 163 K, 263 K, and 328 K. Each mode was given its zero point energy (zpe), a Boltzmann sampling of vibrational levels, and a random sign for its initial velocity. The random signs were obtained using a random number generator, which was monitored to ensure that true randomization was being obtained. A Boltzmann sampling of translational energy was given to the mode correlated to the approach of the O_1 toward the alkene carbons, C_1 and C_2. Until either product was formed, 1-fs steps were taken employing a Verlet algorithm with all atomic motions freely variable. The overall results for the trajectory runs and the resulting KIE predicted from the ratio of products, k_H/k_D, at each temperature is listed in Table 3.

Table 3. Trajectory runs at a variety of temperatures and their respective isotope effects.

T (K)	Runs	H	D	KIE
0	726	422	304	1.39
77	706	409	297	1.38
163	663	387	276	1.40
263	257	149	108	1.38
328	1019	559	460	1.22

An Attempt to Apply Conventional Transition State Theory

A best fit of the Eyring relationship was obtained for the experimentally observed KIEs. Although a less than perfect fit is not unusual, if the reaction selectivity was predictable by transition state theory then the general trends would be comparable. This is not the case at all due to the unusual leveling off at decreasing temperatures observed in the experimental KIEs.

Application of Variational Transition State Theory

From some unusual observations in Lluch's paper on the $^1O_2$ ene reaction of tetramethylethylene-d_6, we suspected that there were errors in the analysis. We have therefore repeated the analysis, particularly using a very careful determination of the minimum-energy path for formation of the H-abstracted versus D-abstracted products. Points on the revised MEP were subjected to a frequency calculation and the resulting harmonic frequencies were used to determine the location and energy of the variational transition state theory bottlenecks for formation of each product at a range of temperatures. From the transition state energies, the isotope effects were calculated in a standard way. The results are summarized in Table 4.

Table 4. Calculated isotope effects for VTST as predicted by Lluch.

T (K)	**KIE**
150	1.207
200	1.160
263	1.126
300	1.111
400	1.087

CHAPTER III

EXPERIMENTAL

General

Isobutyric acid, 99% (Aldrich); butyllithium, 2.5 M solution in hexanes (Aldrich); diisopropylamine, 99% (Aldrich); acetone-d_6, 99.5% (Aldrich); hydrochloric acid, 12 M (EMD); benzenesulfonyl chloride, 99% (Aldrich); pyridine (EMD), diethyl ether (Fisher), Rose Bengal (Lancaster), sodium borohydrate (EM), trifluoromethane (SynQuest), and chlorodifluoromethane (SynQuest) were used without further purification. Tetrahydrofuran (Fisher) and methanol (Fisher) were dried by distillation before use. The butyllithium was titrated versus menthol in toluene using 1,10-phenanthroline as indicator

Synthesis of *gem*-tetramethylethylene-d_6 (9)

2,2-Dimethyl-3-hydroxy-3-(trideuteriomethyl)-4,4,4-trideuteriobutyric acid (14). *Example Procedure*. Under N_2, a dry flask was charged with a solution of 28.5 g (282 mmol) of diisopropylamine in 30 mL of THF. While stirring continuously, the solution was cooled to –78 °C and 100 mL (250 mmol) of *n*-butyllithium solution (2.5 M in hexanes) was added. The solution was allowed to warm to room temperature and stir continuously for 2 h. The solution was then cooled again to –78 °C and 12.25 g (139 mmol) of isobutyric acid in 10 mL of THF) was added. The solution was allowed to warm to room temperature and react for 2 h. The solution was cooled to 5 °C and 8.70 g (136 mmol) of acetone-d_6 in 15 mL of THF was added, the solution was allowed to warm to room temperature and react for 18 h. The reaction mixture was then poured over ice

and washed 4 times with diethyl ether. The aqueous layer was acidified with 12 N HCl and the excess water was removed under reduced pressure by simple distillation. The remaining organic layer was extracted with diethyl ether, dried with $MgSO_4$, and then vacuum filtered. Excess ether was removed by rotary evaporation and the remaining mixture was rinsed with pentane several times until white crystals formed which were then isolated by vacuum filtration yielding 9.15 g (60.1 mmol) of **14**.

3,3-Dimethyl-4,4-bis(trideuteriomethyl)oxetan-2-one (15). *Example Procedure*. A mixture of 9.15 g (60.1 mmol) of **14** in 50 mL of pyridine was cooled to 5 °C, and 21.4 g (121 mmol) of benzenesulfonyl chloride was added. The flask was sealed, shaken thoroughly, and then placed in a refrigerator overnight. At this time, the reaction was judged complete by NMR analysis of an aliquot. The reaction mixture was combined with several volumes of ice and extracted 3 times with diethyl ether. The combined ether layers were washed with saturated aqueous sodium bicarbonate solution and water, twice each. The organic layer was dried with $MgSO_4$, vacuum filtered, and the excess ether evaporated. The remaining mixture was then rinsed with pentane several times and then vacuum filtered to isolate 5.59 g (41.7 mmol) of **15** as dry, white crystals. Deuterium incorporation was determined to be >99.9% by ESI mass spectroscopy.

***gem*-Tetramethylethylene-d_6 (9).** *Example Procedure*. A 5.58 g (41.6 mmol) sample of **15** was distilled, neat, under a water aspirator at 100 °C to yield 2.16 g (23.9 mmol) of the desired olefin **9** (17.6% yield over 3 steps) and evolving CO_2 at the same time. The isolated TME-d_6 was stored in the freezer to avoid evaporation.

Singlet Oxygen Reaction of 9

Conducted in methanol (193 K to 328 K). *Example Procecdure*. Under an oxygen atmosphere, a mixture of 20 mL of dry methanol, 108 mg (1.20 mmol) of **9**, 10 mg (0.01 mmol) of Rose Bengal, and 4 drops of 1,2-dichloroethane was stirred continuously at 198 K while being irradiated with a 300-W sunlamp. The reaction was monitored by GC and after 30% conversion of the tetramethylene-d_6, the irradiation was discontinued. The mixture was then warmed to 225 K and 40 mg (11 mmol) of $NaBH_4$ was added. After stirring at 225 K for 6 h, the volatiles were removed by vacuum distillation, and the mixture was extracted with 50 mL dichloromethane, rinsed four times with water, dried with $MgSO_4$, and filtered through a small silica plug. The dichloromethane was removed by rotary evaporation aided by rinsing the product three times with 5 mL portions of benzene-d_6.

Conducted in methanol/Freon mixture (118 K to 163 K). *Example Procedure*. Using a liquid nitrogen condenser, 20 mL of chlorodifluoromethane was condensed and transferred into a small flask followed by 148 mg (1.64 mmol) of **9**, 10 mg (0.01 mmol) of Rose Bengal, and 1 mL of dry methanol. The solution was stirred under an oxygen atmosphere at 163 K while being irradiated with a 300-W sunlamp. After 2 h, the irradiation was discontinued. The mixture was then warmed to 225 K and 20 mL of dry methanol was added along with 50 mg (14 mmol) of $NaBH_4$. After stirring at 225 K for 6 h, the solution was worked-up in the same manner as describe above.

Conducted in methanol/liquid nitrogen mixture (77 K). *Example Procedure*. Under an oxygen atmosphere, a mixture of 20 mL liquid nitrogen, 100 mg (1.11 mmol) **9**,

10 mg (0.01 mmol) of Rose Bengal, and 1 mL of dry methanol was stirred continuously at 77 K while being irradiated with a 300-W sunlamp. After 2 h, the irradiation was discontinued. The mixture was then warmed to 225 K and 20 mL of dry methanol was added along with 40 mg (11 mmol) of $NaBH_4$. After stirring at 225 K for 6 h, the solution was worked-up in the same manner as describe above.

NMR Measurements

Each sample was prepared in a 5-mm NMR tube filled with benzene-d_6 to a constant height of 5.0 cm. The ^1H spectra were recorded on either a 400 or 500 mHz NMR, using 8-s delays between 45° pulses, a 3.7496-s acquisition time, and collecting 44,932 points. Multiple measurements were obtained for each sample along with a nondeuterated standard that was subjected to the same reaction conditions. Integrations were determined numerically using a constant integration region for each peak in both the sample and standard. Table 5 lists the average integrations observed for each sample along with its respective standard and their standard deviations. The integrations shown for samples obtained at temperatures ranging from 75 K to 218 K were averaged from six consecutive fids, while integrations for samples obtained at temperatures ranging from 248 K to 328 K were from a single fid. A single fid was deemed sufficient at higher temperatures since the KIE variation between each individual fid of at lower temperatures had an average standard deviation of ±0.0036.

Table 5. Average integrations and standard deviations for each NMR sample and standard.

T (K)	H1	H2	std H2	H3	std H3	H4	std H4
75	1000	1013.20	1.92	3046.90	2.64	3652.12	5.9819
standard	1000	1014.09	1.61	3015.55	2.51	5659.20	7.5052
75 dilute	1000	1013.85	5.46	3099.39	17.0	3763.09	22.2075
standard	1000	998.85	0.48	3020.53	0.94	5893.66	2.7840
118	1000	1028.24	4.81	2953.31	4.88	3578.18	8.1137
standard	1000	1014.09	1.61	3015.55	2.51	5659.20	7.5052
138*	1000	1057.91	17.62	3036.45	56.03	3924.38	82.0718
standard*	1000	1016.96	0.45	2954.26	0.91	6071.90	1.9837
158*	1000	1018.19	8.28	3087.10	25.82	3652.92	35.4348
standard*	1000	1012.90	0.23	2978.57	0.80	5516.70	1.3333
163*	1000	1004.4	0.82	3062.05	3.33	3805.72	5.895
standard*	1000	1000.92	0.49	3011.77	0.49	5876.39	1.3318
193*	1000	1032.30	5.55	2944.40	15.09	3952.17	18.6701
standard*	1000	1016.96	0.45	2954.26	0.91	6071.90	1.9837
208	1000	1033.41	0.98	3035.18	2.06	3717.19	1.5453
standard	1000	1011.58	0.89	3021.89	1.58	5714.17	6.4763
218	1000	1016.46	0.95	3013.56	1.88	3847.10	3.10
standard	1000	1002.59	1.51	3038.33	1.51	5842.73	4.64
248**	1000	1017.49	-	3058.75	-	4176.40	-
standard**	1000	998.868	-	2991.63	-	6025.93	-
276**	1000	1034.23	-	3087.66	-	4329.20	-
standard**	1000	998.868	-	3005.97	-	6025.93	-
298**	1000	1028.47	-	3235.71	-	4482.85	-
standard**	1000	998.868	-	3005.97	-	6066.08	-
313**	1000	1026.82	-	3125.19	-	4569.18	-
standard**	1000	1003.48	-	2987.39	-	5988.69	-
328**	1000	1024.11	-	3154.17	-	4679.30	-
standard**	1000	1003.48	-	2987.39	-	5928.59	-

* baseline corrections were employed

** single fid runs

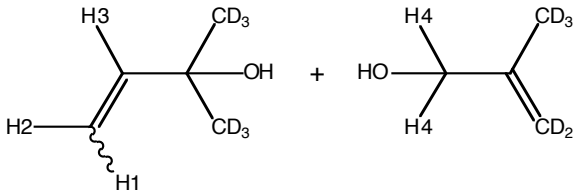

Figure 14. Hydrogen labeling key for KIEs.

From the integrations listed in Table 5 the KIEs were calculated using eq 4 in which H1, H2, H3, and H4 represent the corrected average integrations of the ^{1}H-NMR peaks associated with the four hydrogens as shown in Figure 14. The resulting isotope effects were listed earlier in Chapter II, Table 2.

$$k_H / k_D = \frac{(H1 + H2 + H3)/5}{(H4)/6} \qquad \text{(eq 4)}$$

CHAPTER IV

DISCUSSION

In order to obtain a more comprehensive picture of the temperature dependence of $^1O_2$ with alkenes, each source of data was overlaid for better comparison. Figure 15 is a compilation of the KIEs obtained from the experimental results on tetramethylethylene-d_6, predictions from trajectories, predictions from VTST, and a best-fit Eyring relationship to the experimental data. This compilation allows for the various isotope effects to be examined individually as well as in relation to each other.

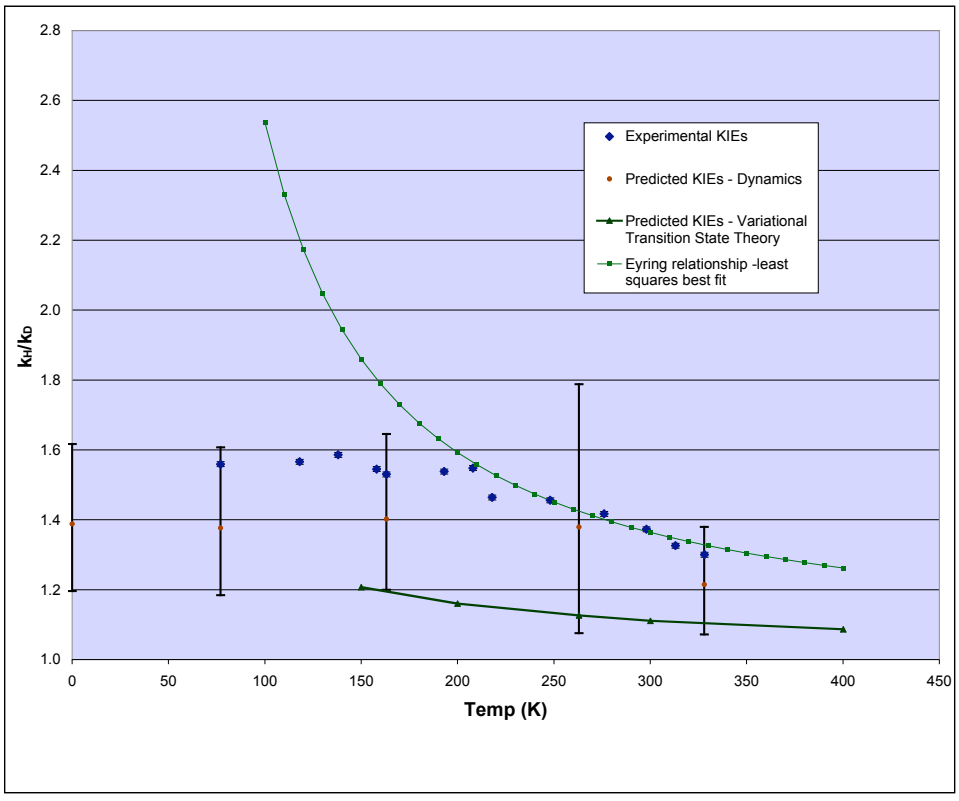

Figure 15. Comparative plot of the KIEs versus temperature for experimentally observed isotope effects, predicted isotope effects from VTST, predicted isotope effects from trajectories, and the best fit Eyring relationship for the experimental KIEs.

The most striking aspect of the experimental results is the trend seen at increasingly lower temperatures, where the KIE begins to level off as it approaches 1.56. Employing constant activation parameters, the Eyring relationship of eq 3 was overlaid to determine the quality of the fit of the selectivity versus temperature. As is apparent in Figure 16, this trend of the experimentally observed KIEs is a completely incompatible fit with the least squares best fit of the Eyring relationship. A perfect fit would not necessarily be expected since activation enthalpies and entropies typically vary with temperature. However, the manner of failure in this case is qualitative in nature, not quantitative, and therefore unique to date.

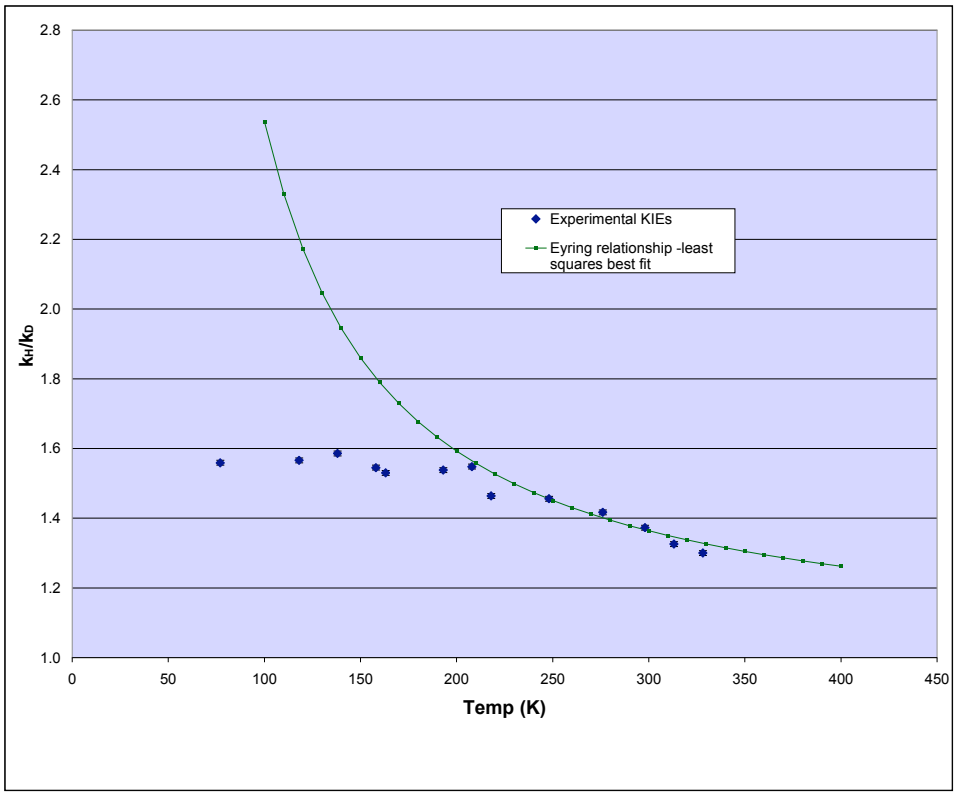

Figure 16. Plot of the experimentally observed intramolecular KIEs and the best-fit Eyring relationship.

When compared to the experimental results, the trajectory predictions are quite remarkable (see Figure 17). At decreasing temperatures, the KIE seems to level off as it approaches a constant value on the order of 1.4. Although they quantitatively underestimate the experimental limiting value of 1.56, the qualitative trends are quite comparable, and all of the experimental results fall within the uncertainty regions inherent to the limited number of trajectories. A consequence of the uncertainty rations is that slight trends would be difficult to discern when predicting the temperature dependence of the selectivity. It is clear, though, that trajectory predictions parallel the experimental observations much more satisfactorily than the Eyring relationship predicted by transition state theory.

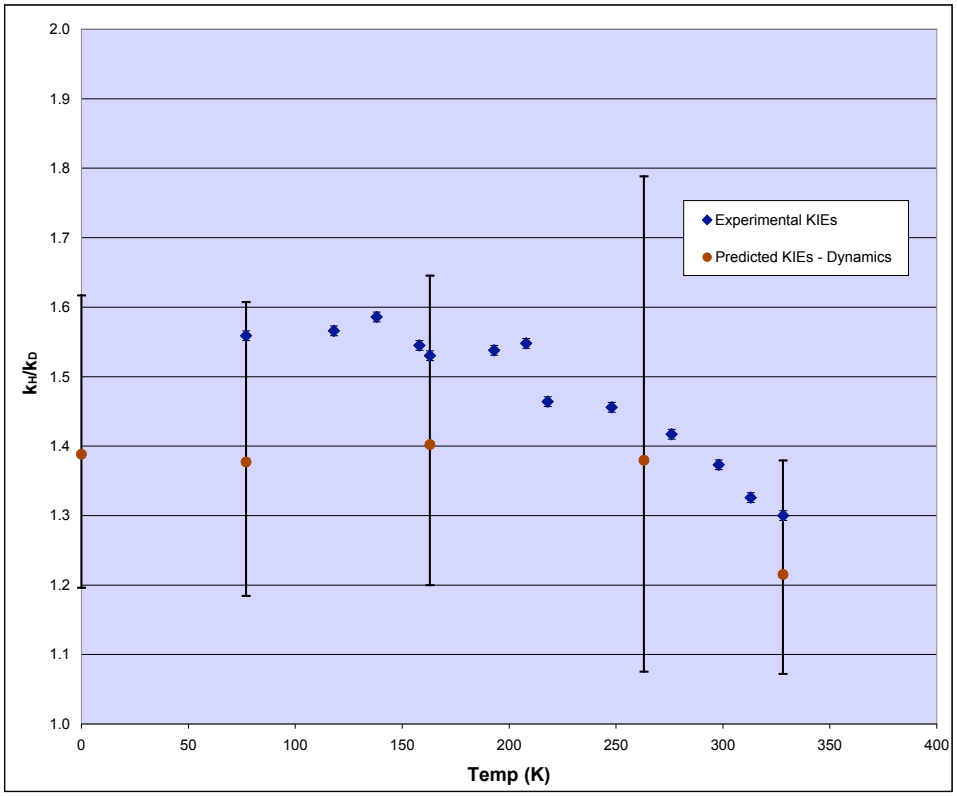

Figure 17. Plot of the experimental KIEs versus dynamic trajectory predictions.

The next step is to compare the predictions Lluch made using VTST (see Figure 18) to the experimental and theoretical work previously described. His predictions substantially underestimate the experimental observations reported in this and previous works, even more so than trajectory predictions. At the time he released his theories, the only experimental observations available were at 263 K and he theorized that the B3LYP potential energy surface used was merely inaccurate, resulting in a quantitative error. In comparison to the Eyring relationship, the trend of Lluch's predictions is comparable, which is to be expected based on shared foundations in transition state theory.

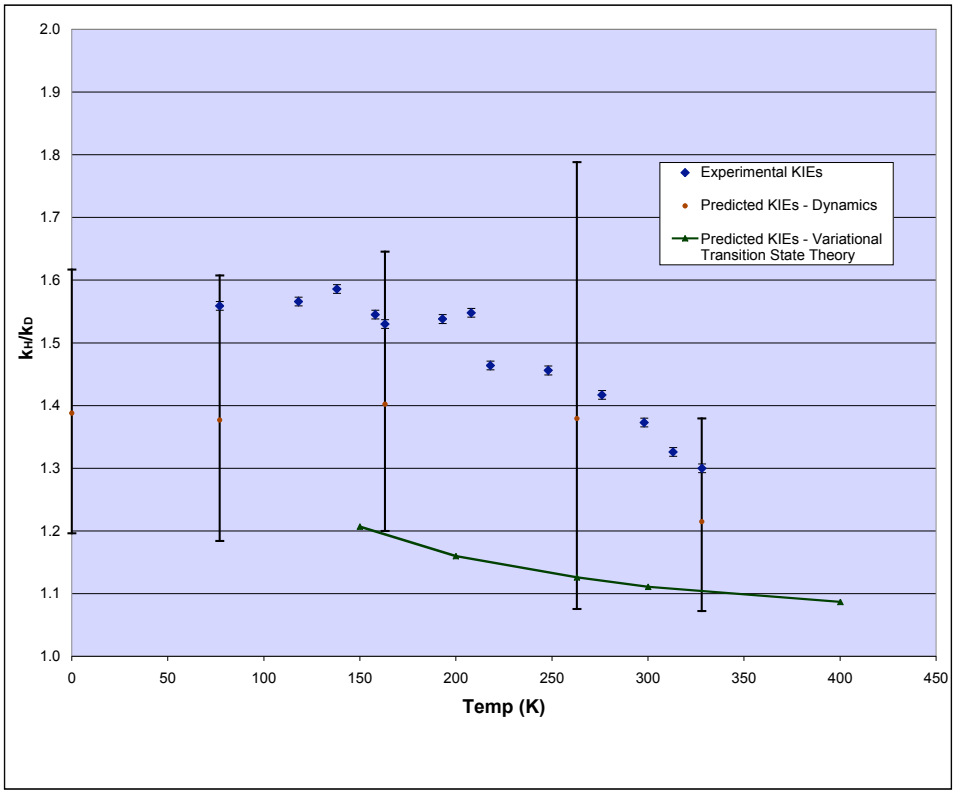

Figure 18. Plot of the intramolecular experimental KIEs, predictions from trajectories, and predictions from VTST.

Conversely, when compared to the experimental observations reported in this thesis the trend is distinctly dissimilar leading to the conclusion that the VTST, like conventional transition state theory, fails to properly predict the selectivity versus temperature on both the quantitative and qualitative level. VTST predicts a symmetrical intermediate in the area near the VRI on the potential energy surface, which then leads to two distinct transition states leading to their prospective products, in the same manner as conventional transition state theory. From the failure of both of these theories to adequately predict the selectivity it can be concluded that an intermediate, as suggested, is very unlikely.

Examination of the potential energy surface for the ene reaction of $^1O_2$ with tetramethylethylene-d_6 reveals a symmetrical surface in Cartesian coordinates, but when examined after the inclusion of zpe the surface appears unsymmetrical. However, this asymmetry does not appear to be a sufficient explanation of the selectivity observed experimentally and more importantly it does not explain the leveling out of the isotope effect at lower temperatures. This leads to the conclusion that the typical effect of zpe on barriers, as described in transition state theory, is irrelevant to the isotope effects observed. The selectivity seems more directly related to the inherent asymmetry in the mass-weighted surface and that of the vibrational modes, which are not implicitly accounted for in transition state theory. This is not to mean that zpe is to be completely ignored, but should be included in a more complete picture of the motion of the atoms. The effects of zpe, as well as thermal excitation, on the vibrational modes can collectively be accounted for from a quasiclassical dynamic standpoint. The contribution

from thermal excitation at higher temperatures is significant, leading to greater atomic motion and decreased selectivity. Conversely, at lower temperatures the contribution from thermal excitation becomes increasingly less significant until the atomic motion is completely ruled out by zpe. In such case the selectivity then becomes independent of temperature, as seen in the leveling off of the isotope effect, since zpe itself is independent of temperature. Although this is not an end-all, all-inclusive explanation of the ene reaction of $^1O_2$ on small alkenes, it is a powerful step towards a better understanding dynamic effects on the selectivity of such systems.

CHAPTER V

CONCLUSION

The experimental KIEs reported in this work present reasonably strong evidence concerning the nature of the mechanism of the ene reaction of $^1O_2$ with gem-tetramethylethylene-d_6. It has been suggested previously by Singleton that this mechanism demonstrates a new form of isotope effect, the characteristics of which are not fully understood. The selectivity observed for this reaction across a broad temperature range is clearly a non-Eyring distribution and thus the mechanism cannot be adequately described solely using transition state theory or even some variation of it. The leveling off of the isotope effect observed at low temperatures was the primary indication of this unique failure of transition state theory to adequately model a reaction of this type. Quasiclassical trajectories runs were found to be much more satisfactory in qualitatively predicting the observed KIEs. They showed that two transition states could exist next to each other on a potential energy surface without a stabilizing intermediate. In such a case as this the selectivity for product formation occurs at the VRI, *before* the second transition state, subsequently making selectivity independent of either transition state. This model is not only theoretically sound, but qualitatively successful in predicting the selectivity observed. Conversely, the VTST model employed by Lluch failed to properly predict the selectivity on both a quantitative and qualitative level. Overall, this is exciting and conclusive evidence of a new isotope effect as suggested previously. There is currently only a modest understanding of the basic characteristics of this new phenomenon, however this work is a major step in coming to a fuller understanding of its existence and distinctiveness.

REFERENCES

(1) Caldin, E. F. *Chem. Rev*. **1969**, *69*, 135-156.

(2) Stern, M. J.; Weston, R. E., Jr. *J. Chem. Phys*. **1974**, *60*, 2803-2807.

(3) Brunton, G.; Griller, D.; Barclay, L. R. C.; Ingold, K. U. *J. Am. Chem. Soc*. **1976**, *98*, 6803-6811.

(4) Hudson, R. L.; Shiotani, M.; Williams, F. *Chem. Phys. Lett*. **1977**, *48*, 193-196.

(5) Zuev, P. S.; Sheridan, R. S.; *J. Am. Chem. Soc*. **1994**, *116*, 4123-4124.

(6) Garcia-Garibay, M. A.; Gamarnik, A.; Bise, R.; Pang, L.; Jenks, W. S. *J. Am. Chem. Soc*. **1995**, *117*, 10264-10275.

(7) Jonsson, T.; Glickman, M. H.; Sun, S.; Klinman, J. P. *J. Am. Chem. Soc*. **1996**, *118*, 10319-10320.

(8) Campos, L. M.; Warrier, M. V.; Peterfy, K.; Houk, K. N.; Garcia-Garibay, M. A. *J. Am. Chem. Soc*. **2005**, *127*, 10178-10179.

(9) Metiu, H.; Ross, J.; Silbey, R.; George, T. F. *J. Chem. Phys*. **1974**, *61*, 3200-3209.

(10) Valtazanos, P.; Ruedenberg, K. *Theor. Chim. Acta* **1986**, *69*, 281-307.

(11) Kraus, W. A.; DePristo, A. E. *Theor. Chem. Acta* **1986**, *69*, 309-322.

(12) Windus, T. L.; Gordon, M. S.; Burggraf, L. W.; Davis, L. P. *J. Am. Chem. Soc*. **1991**, *113*, 4356-4357.

(13) Hrovat, D. A.; Borden, W. T. *J. Am. Chem. Soc*. **1992**, *114*, 5879-5881.

(14) Yanai, T.; Taketsugu, T.; Hirao, K. *J. Chem. Phys*. **1997**, *107*, 1137-1146.

(15) Caramella, P.; Quadrelli, P.; Toma, L. *J. Am. Chem. Soc*. **2002**, *124*, 1130-1131.

(16) Zhou, C.; Birney, D. M. *Org. Lett*. **2002**, *4*, 3279-3282.

(17) Yamataka, H.; Aida, M.; Dupuis, M. *Chem. Phys. Lett*. **1999**, *300*, 583-587.

(18) Bakken, V.; Danovich, D.; Shaik, S.; Schlegel, H. B. *J. Am. Chem. Soc*. **2001**, *123*, 130-134.

(19) Mann, D. J.; Hase, W. L. *J. Am. Chem. Soc*. **2002**, *124*, 3208-3209.

(20) Zhou, C.; Birney, D. M. *Org. Lett.* **2002**, *4*, 3279-3282.

(21) Singleton, D. A.; Hang, C.; Szymanski, M. J.; Meyer, M. P.; Leach, A. G.; Kuwata, K. T.; Chen, J. S.; Greer, A.; Foote, C. S.; Houk, K. N. *J. Am. Chem. Soc.* **2003**, *125*, 1319-1328.

(22) Ussing, B. R.; Singleton, D. A. *J. Am. Chem. Soc.* **2005**, *127*, 2888-2899.

(23) Bekele, T.; Lipton, M. A.; Singleton, D. A.; Christian, C. F. *J. Am. Chem. Soc.* **2005**, *127*, 9216-9223.

(24) Singleton, D. A.; Hang, C.; Szymanski, M. J.; Greenwald, E. E. *J. Am. Chem. Soc.* **2003**, *125*, 1176-1177.

(25) Valtazanos, P,; Elbert, S. T.; Ruedenberg, K. *J. Am. Chem. Soc.* **1986**, *108*, 3147-3149.

(26) Windus, T.L.; Gordon, M. S.; Burggraf, L. W,; Davis, L. P. *J. Am. Chem. Soc.* **1991**, *113*, 4356-4357.

(27) Ramquet, M. N.; Dive, G.; Dehareng, D. *J. Chem. Phys.* **2000**, *112*, 4923-4934.

(28) Taketsugu, T.; Kumeda, Y. *J. Chem. Phys.* **2001**, *114*, 6973-6982.

(29) Caramella, P.; Quadrelli, P.; Toma, L. *J. Am. Chem. Soc.* **2002**, *124*, 1130-1131.

(30) Reyes, M. B.; Carpenter, B. K. *J. Am. Chem. Soc.* **2000**, *122*, 10163-10176.

(31) Stephenson, L. M.; Grdina, M. J.; Orfanopoulos, M. *Acc. Chem. Res.* **1980**, *13*, 419-425.

(32) Grdina, M. J.; Orfanopoulos, M.; Stephenson, L. M. *J. Am. Chem. Soc.* **1979**, *101*, 3111-3112.

(33) Seymour, C. A.; Greene, F. D. *J. Org. Chem.* **1982**, *47*, 5226-5227.

(34) Orfanopoulos, M.; Smonou, I; Foote, C. S. *J. Am. Chem. Soc.* **1990**, *112*, 3607-3614.

(35) Singleton, D. A.; Thomas, A. A. *J. Am. Chem. Soc.* **1995**, *117*, 9357-9358.

(36) Gonzalez-Lafont, A.; Moreno, M.; Lluch, J. M. *J. Am. Chem. Soc.* **2004**, *126*, 13089-13094.

(37) Cheng, C.; Seymour, C. A.; Petti, M. A.; Greene, F. D. *J. Org. Chem.* **1984**, *49*, 2910-2916.

VITA

Name: N. Rebecca Ruiz

Address: Department of Chemistry
Texas A&M University
P.O. Box 30012
College Station, TX 77842

Email Address: ruiz@tamu.edu
rweikel@gmail.com

Eduacation: Northwest Nazarene University
Nampa, ID
B.S. Chemistry
December 2002

Texas A&M University
College Station, TX
M.S. Chemistry
December 2006